Downloaded from orbit.dtu.dk on: Apr 18, 2025

DTU Library

The steel–concrete interface

Angst, Ueli M.; Geiker, Mette Rica; Michel, Alexander; Gehlen, Christoph; Wong, Hong; Isgor, O. Burkan; Elsener, Bernhard; Hansson, Carolyn M.; Francois, Raoul; Hombostel, Karla

Total number of authors:
17

Published in:
Materials and Structures

Link to article, DOI:
10.1617/s11527-017-1010-1

Publication date:
2017

Document Version
Publisher's PDF, also known as Version of record

Link back to DTU Orbit

Citation (APA):
Angst, U. M., Geiker, M. R., Michel, A., Gehlen, C., Wong, H., Isgor, O. B., Elsener, B., Hansson, C. M., Francois, R., Hombostel, K., Polder, R., Alonso, M. C., Sanchez, M., Correia, M. J., Criado, M., Sagüés, A., & Buenfeld, N. (2017). The steel–concrete interface. *Materials and Structures*, *50*(143). https://doi.org/10.1617/s11527-017-1010-1

General rights
Copyright and moral rights for the publications made accessible in the public portal are retained by the authors and/or other copyright owners and it is a condition of accessing publications that users recognise and abide by the legal requirements associated with these rights.

- Users may download and print one copy of any publication from the public portal for the purpose of private study or research.
- You may not further distribute the material or use it for any profit-making activity or commercial gain
- You may freely distribute the URL identifying the publication in the public portal

If you believe that this document breaches copyright please contact us providing details, and we will remove access to the work immediately and investigate your claim.

Materials and Structures (2017) 50:143
DOI 10.1617/s11527-017-1010-1

ORIGINAL ARTICLE

The steel–concrete interface

Ueli M. Angst · Mette R. Geiker · Alexander Michel · Christoph Gehlen · Hong Wong · O. Burkan Isgor · Bernhard Elsener · Carolyn M. Hansson · Raoul François · Karla Hornbostel · Rob Polder · Maria Cruz Alonso · Mercedes Sanchez · Maria João Correia · Maria Criado · A. Sagüés · Nick Buenfeld

Received: 8 December 2016 / Accepted: 31 January 2017
© The Author(s) 2017. This article is published with open access at Springerlink.com

Abstract Although the steel–concrete interface (SCI) is widely recognized to influence the durability of reinforced concrete, a systematic overview and detailed documentation of the various aspects of the SCI are lacking. In this paper, we compiled a comprehensive list of possible local characteristics at the SCI and reviewed available information regarding their properties as well as their occurrence in engineering structures and in the laboratory. Given the complexity of the SCI, we suggested a systematic approach to describe it in terms of local characteristics and their physical and chemical properties. It was found that the SCI exhibits significant spatial inhomogeneity along and around as well as perpendicular to the reinforcing steel. The SCI can differ strongly between different engineering structures and also between different members within a structure; particular differences are expected between structures built before and after the 1970/1980s. A single SCI representing all on-site conditions does not exist. Additionally, SCIs in common laboratory-made specimens exhibit significant differences compared to

U. M. Angst (✉) · B. Elsener
Institute for Building Materials (IfB), ETH Zurich, Stefano-Franscini-Platz 3, 8093 Zurich, Switzerland
e-mail: uangst@ethz.ch

M. R. Geiker · K. Hornbostel
Department of Structural Engineering, Norwegian University of Science and Technology (NTNU), 7491 Trondheim, Norway

M. R. Geiker · A. Michel
Department of Civil Engineering, Technical University of Denmark (DTU), 2800 Kgs. Lyngby, Denmark

C. Gehlen
Centre for Building Materials (cbm), Technical University Munich, Baumbachstr. 7, 81245 Munich, Germany

H. Wong · N. Buenfeld
Concrete Durability Group, Department of Civil and Environmental Engineering, Imperial College London, London SW7 2AZ, UK

O. B. Isgor
School of Civil and Construction Engineering, Oregon State University, Corvallis, OR, USA

C. M. Hansson
Department of Mechanical and Mechatronics Engineering, University of Waterloo, Waterloo, ON N2L 3G1, Canada

R. François
LMDC, INSA, UPS, Université de Toulouse, Toulouse, France

R. Polder
TNO Technical Sciences/Structural Reliability, Delft, The Netherlands

R. Polder
Delft University of Technology, Civil Engineering/ Materials and Environment, Delft, The Netherlands

Published online: 27 February 2017

engineering structures. Thus, results from laboratory studies and from practical experience should be applied to engineering structures with caution. Finally, recommendations for further research are made.

Keywords Steel–concrete interface · Interfacial transition zone · Durability · Corrosion · Inhomogeneity · Variability

1 Introduction

The steel–concrete interface (SCI) influences the structural behavior and durability performance of reinforced concrete, and thus, plays an important role in engineering of reinforced concrete structures. The SCI has a particular influence on the corrosion behavior in chloride exposure environments and in the case of carbonation. It also influences certain aspects of the bond between steel and concrete such as adhesion between steel and concrete, which is particularly important in the case of smooth reinforcing steel where mechanical interlocking does not exist.

Some of the large uncertainties in durability engineering—particularly in explaining and forecasting initiation of chloride-induced corrosion—can be traced to insufficient understanding of the influence of local characteristics of the SCI [1, 2]. To name a few prominent examples, pores, voids, and cracks have been observed to strongly influence initiation of chloride-induced corrosion under some conditions [3–10], but seem to have no influence under other conditions [9, 11]. There are many other characteristics at the SCI that may, or may not, occur locally and that may potentially influence the local susceptibility of the reinforcement to corrosion initiation. A systematic overview and detailed documentation of these, however, are lacking.

This contribution summarizes the state-of-the-art concerning the occurrence—both on-site and in laboratory experiments—of different local characteristics at the SCI, and describes their physical and chemical properties. The influence of these local characteristics on corrosion initiation will be addressed in a separate publication.

The present paper was prepared by members of RILEM TC 262-SCI and is to a large extent based on the presentations and discussions during the first five TC meetings. This paper focuses on conventional carbon steel reinforcement in Portland cement based concrete, leaving considerations of coated, alloyed or high-strength steels as well as other binder types for future treatment. Additionally, the influences of repair techniques (electrochemical remediation, e.g. cathodic prevention and protection) and of corrosion inhibitors and other chemical admixtures on the SCI are excluded in this work. This paper describes the SCI in the hardened concrete after initial cement hydration and steel passivation, but before corrosion has initiated, i.e. it considers the SCI of passive steel during the so-called initiation stage (Fig. 1). The time scale of this stage often forms a substantial part of the service life of engineering structures.

2 Documented characteristics at the SCI

2.1 Terminology and conceptual description of the SCI

Table 1 lists features that are known to occur at the SCI both in laboratory specimens and in engineering structures. We suggest “local characteristics” as a general term to embrace all the individual features and their *local* properties. Note that the term “local characteristics” may refer to both local differences with increasing distance from the steel surface (perpendicular to steel surface) and to local differences across the steel surface, both along the reinforcing steel bar and along its circumference.

M. C. Alonso · M. Sanchez
Institute of Construction Science Eduardo Torroja-CSIC, Serrano Galvache 4, 28033 Madrid, Spain

M. J. Correia
Materials Department, National Laboratory for Civil Engineering (LNEC), Av. Do Brasil, 101, 1700-066 Lisbon, Portugal

M. Criado
Department of Materials Science and Engineering, The University of Sheffield, Sir Robert Hadfield Building, Sheffield S1 3JD, UK

A. Sagüés
Department of Civil and Environmental Engineering, University of South Florida, 4202 E. Fowler Avenue, Tampa, FL 33620-5350, USA

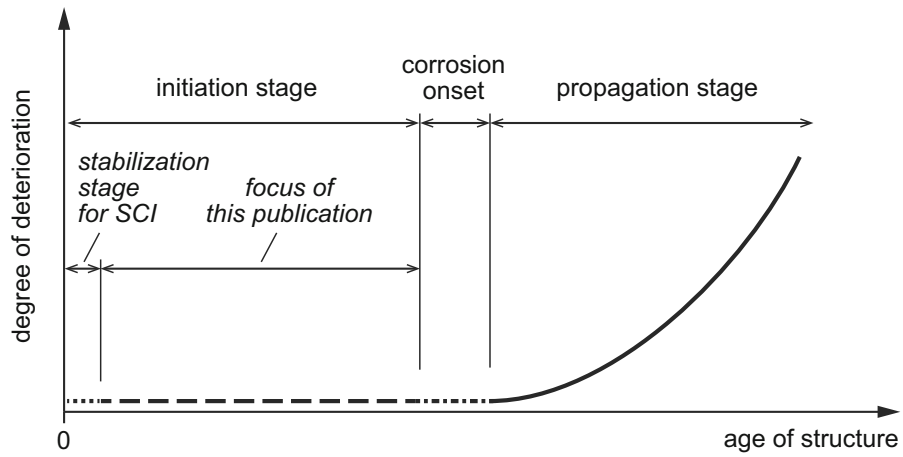

Fig. 1 Schematic illustration showing the stage in the service life of a reinforced concrete structure during which the steel–concrete interface (SCI) is considered in this work

Figure 2 shows some selected characteristics of the SCI; for reasons of clarity it is not possible to display all features listed in Table 1. We found it useful to divide the local characteristics into those inherent to the reinforcing steel bar (steel part of the SCI) and those in the concrete adjacent to the steel (concrete part of the SCI). This classification, however, does not mean that we consider these parts independent of each other. There are obvious interactions when reinforcing steel bars are embedded in concrete as will be discussed in Sect. 3.2. In terms of length scales, we divide the local characteristics into macroscopic and microscopic features. In agreement with various dictionaries, we define "macroscopic" as something "observable by the naked eye". The resolution of the human eye in close reading distance is of the order of 50–100 micrometers [12]. Thus, "microscopic" refers to dimensions smaller than this.

2.2 Reinforcing steel

From the beginning of construction with reinforced concrete in the late nineteenth century, a wide variety of reinforcing steels has been used. Metallurgy and rebar geometry have changed substantially over time due to the increased requirements for mechanical properties and historical evolution of manufacturing processes [13]. Today, across Europe, approx. 200 different steel grades exist, which vary in terms of yield and tensile strength (R_e and R_m), elongation at ultimate strength (A_{gt}) and hardening ratio (R_m/R_e). According to the characteristic yield strength—that varies between 370 MPa and 600 MPa within Europe—reinforcing steel is classified into strength grades, where for example the value 500 in the class B500 represents the characteristic yield strength of the rebar of 500 MPa [14]. Reinforcing steel is also classified according to its elongation at ultimate strength and depending on the hardening ratio, where three different ductility classes for steel reinforcing bars are defined. The classes "A", "B" and "C" belong to A_{gt} higher than 2.5, 5.0 and 7.5% and by hardening ratios higher than 1.05, 1.08 and between 1.15 and 1.35, respectively.

Different methods can be used to satisfy the strength and ductility requirements for construction standards, and these have led to differences in steel microstructure [15–17]. Established processes are micro-alloying (MA), cold working (CW), stretching (STR), and thermomechanical strengthening, e.g. the TempCore® process (TEMP). In thermomechanical strengthening, the steel is immediately and rapidly quenched on the surface by spraying water after the last hot rolling sequence. Following this treatment, the steel is exposed to air cooling. Within this period the martensitic quenched layer is tempered by the preserved heat from the core. Thermomechanical strengthening thus leads to a composite microstructure (Fig. 3) with a tempered martensite surface layer and a more ductile ferrite/pearlite core [15–18]. The classic hot-rolled and cold-worked, as well as micro-alloyed, reinforcing steel bars, on the other hand, have a relatively uniform microstructure across the cross section. Work-hardening by means of cold deforming typically starts from the ferrite-pearlite type of microstructures, which are maintained during the

Table 1 List of local characteristics at the steel–concrete interface (SCI)

Characteristics	Length scale		Influenced by			Occurrence	
	Perpendicular to steel surface	Along steel surface	Steel	Concrete	Exp.	Lab	On-site
Reinforcing steel							
Microstructure and chemical composition	µm	µm	Y	N	N	Y	Y
Lattice defects such as due to cold deformation/work hardening	µm	µm	Y	N	N	Y	Y
Rebar geometry (ribs, Ø, etc.) and rebar orientation	mm	mm	Y	N	N	Y	Y
Welding points	mm	mm	Y	N	N	(N)	Y
Nonmetallic inclusions	µm	µm	Y	N	N	Y	Y
Steel surface							
Steel surface roughness	µm	µm–cm	Y	N	N	Y	Y
Presence/absence of mill scale(s)	µm	µm–cm	Y	N	N	(Y)	Y
Presence/absence of native corrosion products	µm	µm–cm	Y	N	N	(Y)	Y
Chemical composition of mill scale and native corrosion products, including ageing/transformation in the concrete	µm	µm–cm	Y	Y	Y	(Y)	Y
Flaws in mill scale and native corrosion products (cracks, crevices)	µm	µm–mm	Y	N	Y	(Y)	Y
Passive film morphology and composition	nm	µm–cm	Y	Y	Y	Y	Y
Concrete microstructure at the SCI							
Phases present	µm	µm–cm	N	Y	Y	Y	Y
Pore structure	µm	µm–cm	Y	Y	Y	Y	Y
Amount and chemistry of electrolyte in pore structure at SCI			(N)	Y	Y	Y	Y
Macroscopic voids at the SCI							
Entrapped/entrained air voids	µm–mm	µm–mm	(Y)	Y	N	Y	Y
Bleed-water zones, depending on rebar orientation	µm–mm	µm–mm	Y	Y	N	Y	Y
Cracks (including slip/separation)	µm–mm	µm–cm	Y	Y	Y	(Y)	Y
Honeycombs	mm–cm	mm–cm	N	Y	N	(N)	Y
Amount and chemistry of electrolyte in macroscopic voids at SCI			(N)	(Y)	Y	Y	Y
Precipitates and other solids in macroscopic voids			Y	Y	Y	Y	Y
Miscellaneous possible local characteristics at the SCI							
Neighboring/intersecting rebars	µm–mm	µm–cm	Y	N	N	(N)	Y
Tie wires	µm–mm	µm–mm	Y	N	N	(N)	Y
Spacers in the concrete cover (contacting the steel)	µm–mm	µm–mm	N	Y	N	(N)	Y
Metallic or plastic ducts from post-tensioning systems	mm	mm	N	N	N	N	Y
Contamination on steel surface, e.g. grease, oil, etc.	µm	µm–cm	Y	N	N	(N)	Y
Previously deposited concrete splatter	mm	mm–cm	Y	Y	N	N	Y
Foreign matter, e.g. timber pieces, other metallic pieces, metallic deposits from nearby welding, etc.	mm	mm–cm	Y	Y	N	N	Y
Exposure related influences (during service life)							
Moisture and moisture changes							
Temperature and temperature changes							
Chemical exposure, a. o. affecting the chloride concentration/content at SCI							
Structural loads, mechanical stresses							

Symbols Y (yes) and N (no) indicate whether or not these characteristics are influenced by the reinforcing steel (including its surface state at the time of concrete casting), by the concrete (including mix proportions, execution, hardening, curing, ageing, etc.), and/or by the exposure related influences during the service life listed below. Columns "lab" and "on-site" indicate where these characteristics occur primarily

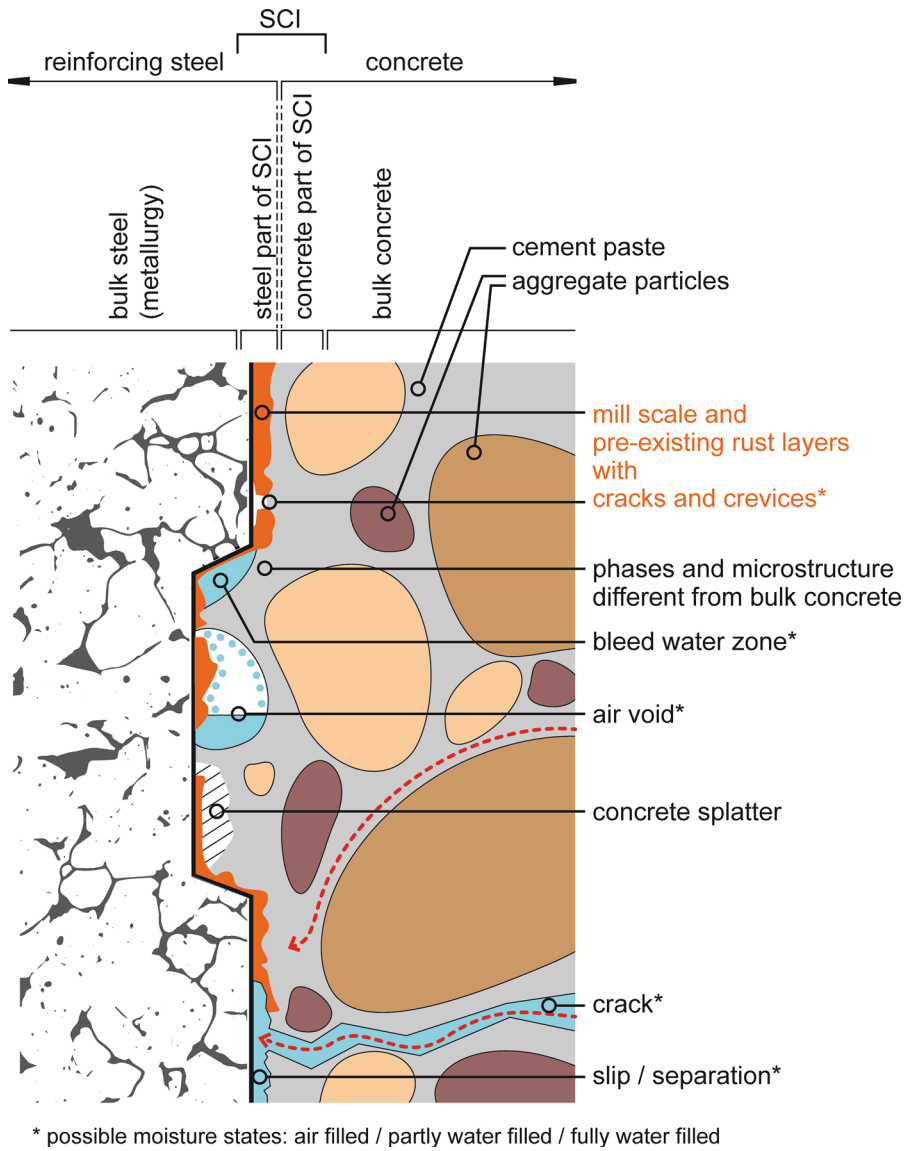

Fig. 2 Schematic illustration of selected characteristics at the steel–concrete interface (SCI) that may or may not be present locally. *Red dashed lines* indicate preferential pathways for chloride ingress; *blue dots* represent adsorbed water (only shown for large pores). Water in cement paste not shown. (Color figure online)

process. Microalloyed steels often consist of a ferritic base matrix. All these microstructures will differ in terms of grain size, nonmetallic inclusions and impurities, which may affect the susceptibility to corrosion [19]. Additionally, the composite microstructure of thermomechanically strengthened rebars also exhibit residual stresses [20, 21] that may affect the resistance to corrosion. In addition, steel in concrete structures is usually stressed due to the structural loading. In typical laboratory investigations, however, the reinforcing steel is generally not under load.

It is important to note that, until approx. the 1980s, predominantly cold-work strengthened reinforcing steel was used. Subsequently, this was replaced by thermomechanically strengthened reinforcing steel in Europe and many other regions of the world. This applies particularly for steels satisfying higher ductility requirements, such as classes B500B and B500C according to [14]. It should be noted also, that nowadays in Europe, virtually all reinforcing steel is produced from recycled materials, while in other regions of the world, e.g. China, a substantial part of the steel is produced from virgin iron ore. This influences the chemical composition of the final product, e.g. impurities such as copper. In other words, older structures were generally built with

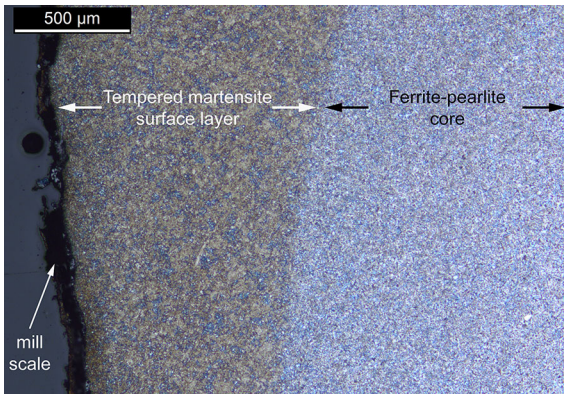

Fig. 3 Non-uniform steel microstructure over the cross section of thermomechanically strengthened reinforcing steel; close up at 9 o'clock position of a polished and etched rebar section (photograph courtesy of Ueli Angst, ETH Zurich, Switzerland)

different types of reinforcing steel, in terms of microstructure, than structures built over the last 20–30 years.

Reinforcing steel in recent structures not only differs strongly from that in older structures in terms of microstructure, chemical composition and mechanical properties, but also with respect to rebar geometry. Up to ca. 1925, primarily smooth/plain rebar steel of round or square cross section was used [13]. Later on, to improve bond and anchorage, a wide variety of irregular (rather than smooth) rebar surface geometries were marketed, including cold twisted square bars, and various corrugated and deformed bars. For instance, European standard EN 10800 distinguishes between "ribbed steel" and "indented steel" and stipulates tolerances for the dimensions and number of ribs and indentations, respectively [14]. The bar geometry (location and shape of ribs or indentations, etc.) may influence the SCI, e.g. by causing local bleed water zones under ribs or between indentations (refer to Sect. 2.5.2) and by defining the location of cracking (refer to Sect. 2.5.3).

2.3 Reinforcing steel surface

2.3.1 General remarks on the different zones along the reinforcement surface

Along the surface of the reinforcing steel there may be different zones, namely bare steel, steel covered with mill scale or with pre-existing (native) rust layers. Once these zones come in contact with the alkaline pore solution of the concrete, different chemical and electrochemical reactions will occur, depending on the zone (bare steel, mill-scale, rust) in contact with the pore solution. As long as the solution is alkaline (and free from chlorides), native iron oxide/hydroxide layers such as mill scale and initial corrosion products are either thermodynamically stable or may undergo transformation towards more hydrated compounds. This depends also on the concentration of dissolved oxygen in the pore solution. In alkaline and chloride free solutions, bare steel surfaces will undergo passivation, i.e. a protective passive film of some nanometer thickness will be formed on the steel surface. Such bare steel surfaces may be found exposed between zones coated with mill scale or native corrosion products, or exposed in crevices within these.

2.3.2 Mill scale

During hot rolling at the steel mill, a so-called mill scale is formed on the reinforcing steel surface [22]. This mill scale consists of iron oxides, typically wüstite (FeO), formed at temperatures above 570 °C. It may also contain magnetite (Fe_3O_4), hematite (α-Fe_2O_3) and maghemite (γ-Fe_2O_3). Mill scale is generally brittle and, thus, during handling, e.g. bending of reinforcing steel bars, it is likely to crack. Mill scale is different from corrosion products in terms of origin and formation, but also with respect to morphology and composition. It is noted that certain rebar treatments (e.g. the Thermex® process) involve a final jetted water quenching step, which may effectively eliminate much of the high temperature scale, leaving only a thin deposit formed at lower temperatures. For cold-work hardened steel, the major part of mill scales will be eliminated during processing.

Ghods et al. [23] investigated the properties of the mill scale on different reinforcing steel bars by means of scanning electron microscopy (SEM) and focused ion beam microscopy. Cross-sectional images showed that the mill scale exhibited a crystalline structure and was deposited on the steel substrate in the form of columnar grains. While on the reinforcing steel from one manufacturer only certain areas of the steel were covered with a relatively thin layer of mill scale (maximum thickness of 2 µm), the steel from other manufacturers was more uniformly coated with mill scale (thickness up to 30–40 µm). Because of their larger thickness, the mill scale and the interface

between steel and mill scale exhibited voids, crevices and cracks. Some of these voids and crevices were connected to the concrete by cracks, which serve as pathways for concrete pore solution to reach the steel surface, hence allowing ion movement between the pore solution and the crevices (Fig. 4). The solution within these cracks and crevices may differ in composition from the concrete pore solution at the crack/crevice opening [23].

Trejo and Monteiro [24] reported that the thickness of mill scales on hot rolled steels ranged from 0 to approx. 20 μm. They also observed cracks in the mill scale.

Wong et al. [25] investigated essentially non-corroded interfaces of reinforcing steel (as-received) embedded in concrete by means of SEM and EDX element mapping. The mill scale had a relatively uniform thickness of 20–50 μm, in agreement with Ghods et al. [23], and was also found to be fractured. EDX spot analysis of the sections indicated that the mill scale consisted mainly of FeO (wüstite), with minor amounts of Fe_3O_4 (magnetite) and Fe_2O_3 (hematite).

Poursaee and Hansson [26] investigated as-received reinforcing steel bars exposed to synthetic pore solution (pH ca. 13.5). Raman spectroscopy indicated that the native oxides (described as mill-scale) consisted primarily of hematite (α-Fe_2O_3) and maghemite (γ-Fe_2O_3).

Mill-scale in contact with concrete is relatively stable. An analysis of the SCI in samples taken from up to 260 years old reinforced concrete structures (or structures based on similar hydraulic binders), partially corroded due to carbonation, revealed the presence of remnants of the initial mill scale at the steel surface [27]. This layer was composed of wüstite, magnetite, and hematite. In some cases, it was covered with an additional layer of more hydrated compounds. These may have been formed either due to partial transformation of mill scale (interacting with the concrete pore solution) or due to aqueous corrosion of the underlying steel. Concerning the latter, a corrosion mechanism was in [27] suggested where ferrous ions released at the steel surface migrate through the mill-scale and precipitate as oxyhydroxides at the outer surface of the mill scale. Similarly, Walsh and Sagüés [28] found well preserved mill scale on much of the surface of rebar extracted from a 60 year old reinforced steel pile submerged in marine water.

In summary, in alkaline and chloride-free concrete transformation of mill scale appears to take place over a long time and remnants of it are likely to be found even after several decades of service life. Nevertheless, this layer of oxides (mainly wüstite, but also magnetite, hematite, and maghemite) offers far less corrosion protection of the underlying steel than a true passive film. This may be explained by the presence of cracks and crevices in the mill scale.

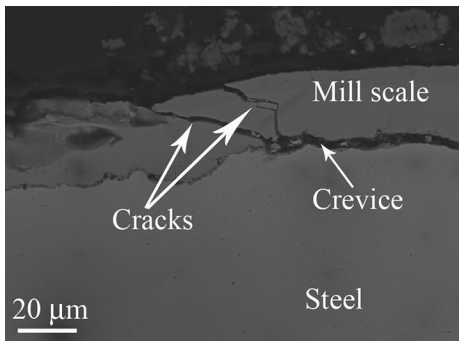

Fig. 4 SEM micrograph of sectioned rebars with mill scale showing cracks and crevices in mill scale (reprinted from [23], with permission from Elsevier)

2.3.3 *Native rust layers*

Once the reinforcing steel leaves the manufacturer, it will experience very different exposure histories, depending on the conditions during transport, handling, and storage. Particularly indoor or sheltered vs. outdoor storage conditions strongly affect the formation of superficial rust layers. Corrosion products may form under atmospheric corrosion conditions, in an adsorbed layer of moisture, or in larger liquid volumes present on the steel surface such as water droplets (rebars exposed to rain, condensation of water) or in cases of (partial) immersion in liquid water. Furthermore, exposure to salt-spray and salt containing aerosols (e.g. when stored on construction sites exposed to marine environment) may give rise to chloride-containing rust layers. These rust layers will likely differ in composition and morphology depending on the exposure conditions and will, most likely, consist of hydroxide layers rather than oxides. Moreover, in contrast to mill scale, the rust layers formed after the steel manufacturing process will not contain significant amounts of wüstite.

Within the work carried out in RILEM TC 235-CTC, rebars were collected from laboratories in 9 different countries, primarily from Europe, in so-called "as-received" condition and tested. These surfaces differed significantly in terms of visual appearance. Furthermore, significant differences in the electrochemical behaviour of these surfaces were observed, depending on the amount of red/brown rust present [19].

Stefanoni et al. [29] measured local open circuit potentials of individual points on the surface of "as-received" reinforcement steels by locally contacting the steel with a test electrolyte and an electrochemical sensor. Surfaces with only black mill-scale or rebars that were severely pre-rusted (entire surface covered with rust) showed a narrow distribution of local open circuit potentials (standard deviation ca. 40 mV) whereas the intermediate situation including both zones of almost bare steel and zones coated with red-brown corrosion products, spanned a large range in terms of local electrochemical properties. While the local open circuit potentials of pre-rusted rebars spanned a range of ca. 200 mV, immersion in an alkaline solution reduced this inhomogeneity to ca. 20 mV within one day (measured after removal from solution) [29]. This indicates relatively fast transformation, i.e. towards more anodic potentials, of the rust and mill-scale initially present on the steel surface when in contact with alkaline electrolyte such as concrete pore solution.

2.3.4 *Passive film*

Formation of passive films The formation of a passive film in alkaline environments of different pH has been mainly studied in solutions by electrochemical techniques. The steel surface was machined [30], ground [31], sandblasted [26, 32] or in most cases mechanically polished [33–37]. Upon exposure to alkaline solutions, literature work agrees on an asymptotical increase of the open circuit potential (OCP) [26, 30–34, 36–40] and of the polarization resistance [32, 37, 38, 40] with time of exposure, indicating the formation of a protective iron oxide film. Although a protective passive film starts to form soon after exposure of steel to passivating solutions, the quality and stability of the film depends on the exposure duration and the chemical composition of the passivating solution. Longer immersion times lead to higher polarization resistance [30, 37, 40]. While at pH > 13, protective properties of the passive film are clearly observed after about 1d of immersion, at least 3–5 days are required for steel in saturated $Ca(OH)_2$ (pH $\sim$ 12.5) [26, 38, 40–42]. However, even for prolonged immersion, saturated $Ca(OH)_2$ solutions may not be representative for concrete pore solutions [40]. Sulfate ions have been shown to have a negative influence on film quality [41].

Structure of passive films Surface analysis has shown that the passive film formed on steel in alkaline solutions has a bi-layer structure [37, 43, 44] with an inner Fe^{2+}-rich oxy-hydroxide (1–3 nm) and an outer Fe^{3+}-rich hydroxide film (5–10 nm), with the overall thickness typically in the range of 3–15 nm [34, 36, 44]. With increasing time of immersion, the outer Fe^{3+} layer of the film increases in thickness, while the inner Fe^{2+} layer remains relatively stable, leading to an observation of increasing ratio Fe^{3+}/Fe^{2+} in the oxide film [34, 37, 38]. This change in Fe^{3+}/Fe^{2+} in the overall passive film has been found to be potential dependent [34, 37, 43] and can lead to a pseudo-capacity when subjected to DC currents or at very low frequencies of AC signals [45]. The higher Fe^{3+} content of the bulk film corresponds to more positive OCP or higher polarization resistances [34, 37]. At typical potentials of passive steel in alkaline, oxygenated concrete, the passive film can be expected to consist mainly of Fe^{3+} oxide and Fe^{3+} oxy-hydroxide [43]. Based on Raman spectroscopy it was in [26, 40] concluded that the passive film composition is similar in concrete pore solutions and in sat. $Ca(OH)_2$. However, Ghods et al. [46] reported the presence of Ca, K, and Na in the passive film from the passivating solutions, suggesting that the pore solution composition may have an influence on the passive film composition and properties.

Protective properties Formation of the passive film leads to a decrease in corrosion rate with time reaching values of <0.1 μA/cm^2 (1 mA/m^2) corresponding to mass loss <1 μm/year, i.e. an insignificant rate [32, 37, 38, 40]. This protective nature of the passive state is associated to a marked decrease in the ionic conduction in the film (ion barrier); a lower electronic conduction was also reported [39]. The passive state is maintained in reinforced concrete structures for a very long time, but may be lost when chloride ions reach the steel. Chloride-induced depassivation has been associated with a change of the oxidation state of the inner

part of the passive film [26, 44, 47] leading to breakdown of the film. As a consequence, experiments that probe the resistance against chloride-induced corrosion should start only after a sufficiently long pre-passivation time that varies according to the pH of the electrolyte [26, 38, 40, 41] (see above). As the onset of chloride-induced corrosion is a local phenomenon it is not yet established if a higher surface-averaged polarization resistance always corresponds to a higher resistance against pitting corrosion.

Influence of structural loads Experimental investigations have shown that passive films formed on steel specimens degrade when subjected to mechanical stresses. Feng et al. [48] performed electrochemical impedance spectroscopy on steel samples while they were immersed in alkaline solutions and simultaneously subjected to mechanical stresses. The polarisation resistance was found to significantly decrease with increasing applied stress. This was explained by cracking and delamination/spalling of the relatively brittle passive film. The results also indicated that passive films are more seriously damaged under compressive stresses than under tensile stresses. The hypothesis is that the passive film buckles and becomes detached over a larger area than when only cracks are formed in the case of tensile stresses. In another study [49] steel samples were first passivated in alkaline solution (pH 12.74) and then exposed to air and subjected to bending leading to tensile stresses in the passive film. This simulates the situation of a reinforced concrete structure under alternating drying/wetting conditions. After loading, the specimens were immersed back in the alkaline solution and repassivation times were measured (in unloaded state). It was found that the steel needed longer times to repassivate when previously subjected to higher mechanical stresses.

2.3.5 Steel surface area and surface roughness

There has been significant research on the corrosion behaviour of metallographically polished surfaces of steel [50–52]. While this is an ideal study of the basic alloy properties, it does not represent the corrosion behaviour of ribbed/indented, as-received reinforcing bars in practice (cf. Sects. 2.3.2 and 2.3.3). Similarly, in recognition of the blurring effects of pre-existing rust layers or mill scale on the results of corrosion tests with reinforcing steels, these oxide/hydroxide layers have also frequently been removed by abrasive blasting (such as sandblasting) [32]. The steel surface thus exposed may appear to be rougher than that of the initial mill scale, at least at some magnification levels, but the blasted steel surface can actually show less ability to sustain cathodic reactions than the mill scale [53]. For steel already scale-free, increasingly finer surface finishes do decrease the amount of effective, exposed steel surface area [54, 55]. Furthermore, abrasive blasting also affects the extent to which individual features on the metal side, such as microscopic occluded regions, may be present. In summary, steel surfaces of rebars in laboratory specimens are, in many cases, not representative for the conditions in engineering structures.

2.4 Concrete microstructure and chemistry at the SCI

Considering that the size of reinforcement is substantially larger than the size of cement grains, the concrete part of the SCI can, as a first approximation, be assumed similar to the interfacial transition zone (ITZ) between cement paste and inert aggregate particles in concrete.

The development of the porosity and dominant phases in the ITZ was described by Scrivener et al. [56]. Not considering execution and bleeding-induced inhomogeneities, the origin of the ITZ is in this paper explained by the so-called ‘wall effect’ causing reduced packing density of the cement grains near to less curved surfaces. The authors describe the ITZ as a region of transition with progressive changes. The effective thickness depends on the feature being studied and on the degree of hydration. The approximate thickness—and the heterogeneity—of the ITZ is comparable to the size of cement grains.

The initial porosity of the ITZ is high compared to the bulk cement paste because of the limited packing of cement grains in this zone. Despite the fact that a higher amount of smaller—and faster reacting—cement grains are present in the ITZ compared with the bulk, and that hydration products—especially $Ca(OH)_2$ but also outer C–S–H and ettringite—tend to precipitate in the ITZ, the porosity of the ITZ appears to remain higher than the porosity of the bulk cement paste.

Comparing the concrete part of the SCI around steel bars with different orientation and the ITZ around

aggregate particles, Horne et al. [57] found increased porosity in the first few μm from the surfaces followed by accumulation of $Ca(OH)_2$ around 5 μm from both steel and aggregate surfaces, except the underside of horizontal bars, where a 40 μm wide porous zone was observed. Microstructural gradients of $Ca(OH)_2$ and porosity in the ITZ around aggregates and the concrete part of the SCI around vertical and topside/underside of horizontal rebars are illustrated in Fig. 5. Slightly more $Ca(OH)_2$ was observed in the vicinity of vertical rebars than at both aggregates and the topside of horizontal rebars, and none was observed within 0–40 μm from the underside of horizontal rebars. In the range of 10–35 μm from the steel surface the $Ca(OH)_2$ content was significantly lower at the topside of horizontal bar than around vertical rebars. Comparing as-received and wire-brushed steel bars, highest $Ca(OH)_2$ contents were found after 1 year around the cleaned rebars. In addition, Horne et al. [57] also observed that especially the underside of ribs on vertical rebars had coarser microstructure than other regions.

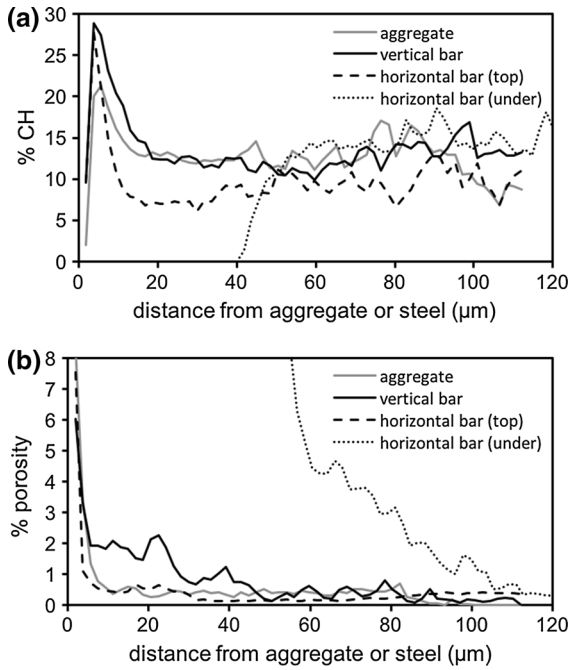

Fig. 5 Microstructural gradients of **a** $Ca(OH)_2$ (CH) and **b** porosity in the ITZ between cement paste and aggregate and the SCI between cement paste and steel bars. Concrete, $w/c = 0.49$, 1 year, 9 mm bars. Acc. to Horne et al. [57]; courtesy of Ian Richardson

Already in 1959 Bäumel [58] described that $Ca(OH)_2$ surrounds the steel in concrete, and in 1975 Page [59] documented the presence of a dense, lime-rich layer of hydration products on the surface of steel in cementitious material. Page suggested that the $Ca(OH)_2$ might buffer the pH in the pore solution and act as a physical barrier. While many investigations have confirmed the presence of lime-rich zones at the SCI [60], Glass et al. [61], found no general indication of preferential formation of $Ca(OH)_2$ at the steel surface and suggested that the hypothesis of a protective layer should be extended to include other solid phases that may buffer the pH.

The binder type may affect the ITZ and the concrete part of the SCI due to differences in packing of the cement grains, their reactivity, and hydration products formed. For example, Gjørv et al. [62] observed that the addition of condensed silica fume (8 or 16% of replacement by mass of Portland cement) reduced both the porosity and the width of the ITZ. This was attributed to reduced bleeding, reduced preferential orientation of $Ca(OH)_2$ crystals and the pozzolanic reaction between silica fume and $Ca(OH)_2$. It was also suggested that the improved initial particle packing is a potential mitigating factor. Larbi [63] describes that after advanced pozzolanic reaction in mortars with addition of silica fume, and fly ash, metakaolin and blast furnace slag the interface in general becomes denser and with practically no visible large crystals of calcium hydroxide.

In addition, the binder type will affect the pore solution composition. A recent paper [64] reviews the impact of supplementary cementitious materials (SCM) on the pore solution composition of cementitious materials. They found pH values in the range of 12.5-14 and that the free alkali content is the main factor controlling pH. Generally, the alkali content decreases with increasing replacement of Portland cement (PC) by SCMs. Blast furnace slag (GGBS) normally contains less alkali than PC and for replacement levels higher than 40% lower pH is usually found in PC-GGBS blends. Reduced pH is also observed for PC-fly ash (FA) blends; partly because the uptake of aluminium in C–S–H facilitates alkali binding.

Upon exposure to penetrating substances, microstructural changes in form of change in type, amount and distribution of solid phases and change in the amount and composition of the pore solution composition might take place. To the authors

knowledge such changes have not been quantified for the SCI. Assuming unlimited exposure to sea water, data from [65] might provide guidance on potential long-term elemental zonation and phase changes. Potential filling of macroscopic pores with solids is discussed in Sect. 2.5.5.

2.5 Macroscopic voids at the SCI

2.5.1 Entrapped and entrained air voids

Air voids at the SCI give rise to marked local differences in terms of physical conditions at the steel surface. This is because of the significant change in characteristics of steel in contact with a matrix of cement paste and aggregates compared to steel in contact with a void (Fig. 6). Air voids at the SCI are produced when rising air bubbles adhere to the surface of bars or become trapped beneath horizontal surfaces of reinforcement steel bars during concrete compaction. Air is commonly present in fresh concrete, in the form of bubbles, either as the result of intentionally entrained or unintentionally trapped air. Air does not mix with the fresh concrete and is thus present in the form of bubbles. These bubbles may strongly differ in size, and—largely depending on their size—also in shape [66].

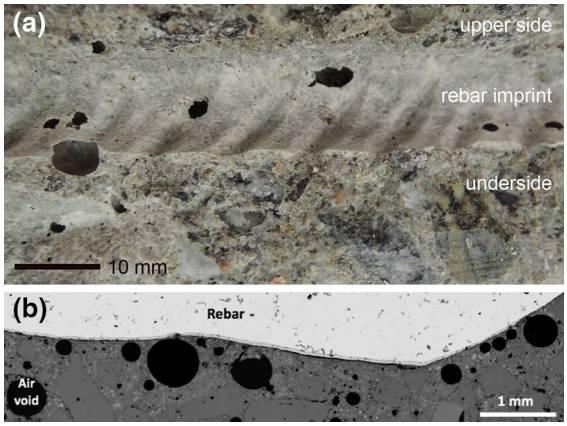

Fig. 6 Air voids at the SCI: **a** macroscopic, irregularly shaped entrapped air voids found in a sample taken from a reinforced concrete tunnel segment (age ca. 40 years) in Switzerland (courtesy of Ueli Angst, ETH Zurich, Switzerland), **b** backscattered electron micrograph showing spherical, entrapped air voids beneath a rebar in concrete (courtesy of Hong Wong, Imperial College London, UK)

Small bubbles such as entrained air voids (typical diameter of 50 μm) have normally a near spherical shape [66, 67]. As such, only a minor part of the spherical void is in contact with the steel surface. Therefore, only a very small portion of these air voids can be seen when the rebar is removed to expose the SCI.

Entrapped air voids are typically >1 mm in diameter. In contrast to entrained air voids, the shape of entrapped air voids can be very irregular. This is partly because their shape is influenced by the contour of surrounding aggregate particles [66].

An important feature of all air voids is that they are initially, due to their origin, not water-filled. However, the moisture state of these voids may change during the service life of a structure and this will be further discussed in Sect. 2.5.4.

There is widespread evidence that interfacial air voids frequently occur in specimens prepared in the laboratory and in engineering structures. In [68], specimens of 20 non-air-entrained and 10 air entrained concrete structures were taken and analysed in the laboratory. It was concluded that the air void system of engineering structures is comparable to that observed in concrete specimens made in the laboratory.

2.5.2 Bleed water zones and voids

As the result of segregation, settlement, and bleeding of fresh concrete, voids can form under horizontal

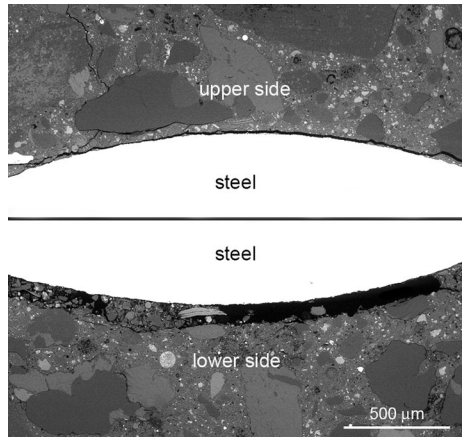

Fig. 7 Bleed water zone at the underside of a rebar; backscattered electron micrograph of polished sections showing upper and lower SCIs in a specimen (Portland cement with 20% fly ash replacement, $w/b = 0.5$, hardened under sealed conditions for 1½ years) (from [9])

reinforcing bars (Fig. 7) [6–9, 57, 69–71]. François et al. [7, 70] found that these defects of the SCI at the underside of the steel increased in relation to the depth of concrete under the steel. However, differences between upper and underside of the rebar were only observed when the concrete depth was larger than 150 mm. Mohammed et al. [71] also observed that gaps were only found under horizontal bars cast in the top part of reinforced elements and not under those cast in the bottom part. This is also known as the "top-bar effect" [70]. In [9], on the other hand, the presence of a bleed water zone was also found when the height of concrete below the steel was only 30 mm. SEM analysis of sections perpendicular to the steel revealed that the bleed-water zone was typically 100–200 μm wide [9]. It consisted largely of a void along the steel surface, interspersed with zones of loosely packed aggregates particles and cement hydration products (Fig. 7). The porosity of these zones was coarse. Similar findings were also made by Horne et al. [57].

Settlement (bulk shrinkage) may cause empty voids at the underside of the reinforcing steel, but a thin layer of paste may adhere onto the rebar surface.

Bleed water may also accumulate at the SCI to form voids of limited lateral dimensions and may appear similar to entrapped air voids. However, bleed water voids have a more elongated nature or crescent shape and are thereby able to achieve a greater contact area with the rebar surface compared with air voids. Another major difference is that they are initially water filled, but can be emptied by chemical shrinkage and upon drying and, therefore, these bleed water voids can be mistaken as entrapped air voids. Empty bleed water voids may be re-filled with water on re-wetting (cf. Sect. 2.5.4).

One implication of bleed water zones is that the direction of casting, particularly when producing laboratory specimens, strongly influences which side of the reinforcing steel exhibits a more porous zone, which may, depending on later direction of chloride ingress, affect the results of corrosion studies.

2.5.3 *Cracks, slip, and separation*

Tensile and/or flexural loading of reinforced concrete can cause complex cracking and deformation behaviors as schematically illustrated in Fig. 8. Once the tensile capacity of the concrete is reached, a load-induced primary crack is formed in the concrete, which is wider at the concrete tensile surface than at the rebar, due to the restraining effect of the reinforcement. The crack usually follows a tortuous path through the cover and can exhibit minimum width within the cover, e.g. as it passes between two closely spaced aggregate particles, and thus can be narrower at the reinforcement than the crack opening at the surface. Upon the formation of primary cracks, internal micro-cracks form around the rebar ribs near the primary crack due to the transfer of tensile load through the rebar ribs into the concrete (causing additional damage at the SCI) and extend with increasing load (Fig. 8a). Upon further loading, internal cracks grow from their tips and reach the concrete surface to be secondary cracks. Finally, at higher steel stresses, longitudinal cracks are initiated near the rebar at the faces of primary cracks and then grow towards the outside of the specimen (Fig. 8b) [72–74]. The crack formation process is, thereby, divided into two phases, the crack formation, and the stabilized cracking phase [75]. The crack formation phase is characterized by the development of random cracks at locally weak sections. During the stabilized cracking phase, no additional cracks are formed and an increase of load causes an increase of crack widths only.

The formation of primary, internal, and secondary cracks is accompanied by damage within the SCI, i.e. slip and separation. Slip relates to a displacement discontinuity between the reinforcement and the surrounding concrete parallel to the reinforcement, while separation corresponds to a displacement discontinuity between the reinforcement and the surrounding concrete perpendicular (in the surface-plane) to the reinforcement. The average crack spacing and, thus, cracking-induced damage along the SCI depends on the reinforcing bar diameter, bond characteristics, concrete strength, concrete cover, the distribution of perpendicular rebars, and effective reinforcement ratio [76]. While crack widths of primary, internal, and secondary cracks range between μm and mm, the extent of these cracks can be up to several meters. Similarly, cracking-induced damage at the SCI (i.e. slip and separation) might be several m in length, while ranging between several μm and mm in width.

2.5.4 *Degree of saturation*

All available literature on the moisture state in concrete is related to bulk concrete rather than to the

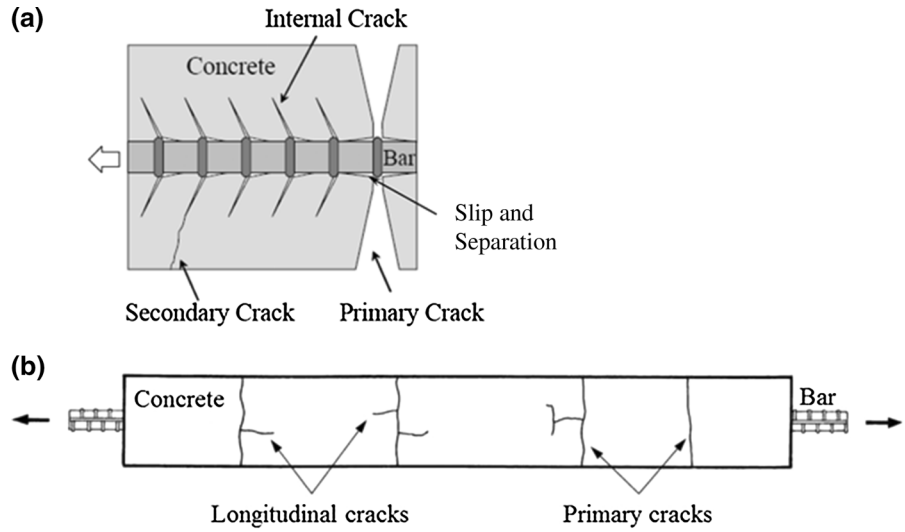

Fig. 8 Schematic illustration of **a** damage and cracking (primary, internal, and secondary cracks) at SCI (after [111]), and **b** primary and longitudinal cracks in concrete under tensile load (after [72]). Figure not to scale

concrete close to the SCI. At the end of the section, possible limitations concerning the application of the data to the SCI are highlighted.

The degree of saturation, S, of concrete depends on the exposure conditions (moisture and temperature) and the pore structure, as well as on the moisture history and pore solution composition. According to Fagerlund [77, 78] moisture in concrete can be divided into three ranges: the hygroscopic range, the capillary range, and the over-capillary range (Fig. 9). The capillary range and over-capillary ranges are not differentiated in most literature, but are combined and referred to as the 'over-hygroscopic range'. However, we will distinguish these ranges in discussing the

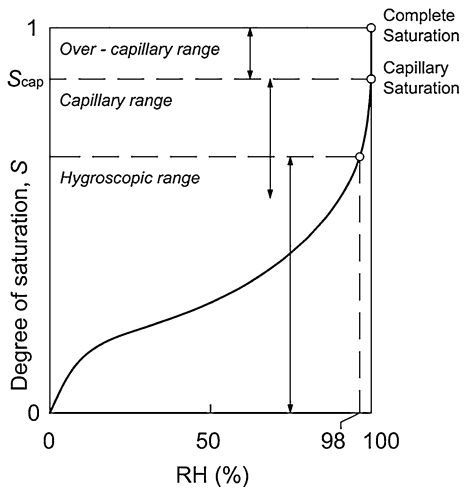

Fig. 9 Adsorption isotherm showing the three moisture ranges in concrete (after [77])

mechanisms of air-void filling. The (governing) mechanisms of water uptake are

- Hygroscopic range (0 to about 98% RH): adsorption and capillary condensation
- Capillary range (up to 100% RH): capillary suction; capillary saturated at $S = S_{cap}$
- Over-capillary range: further saturation due to gradual dissolution of air in the pore water and diffusion to larger pores or the surface; complete saturation (all three ranges) at $S = 1$.

During capillary suction, air bubbles will be trapped in coarse pores surrounded by a network of finer pores [78]. Entrapped air bubbles are exposed to pressure which is inversely proportional to the bubble radius. Due to over-pressure, air bubbles with smaller radius than approximately 10 μm are according to the theory not stable at capillary saturation (and not in fresh paste). Larger bubbles stay initially air-filled, but will contract due to over-pressure and a small water volume will surround the bubble. The volume of water decreases with pore size; for a pore with 10 μm radius the thickness of the initial water film is estimated at 0.25 μm [78]. It is assumed that the walls of air-filled pores will, as a minimum, be covered by a layer of adsorbed water molecules. The layer of adsorbed water molecules on cement hydrates is approximately 1 nm thick [79].

A detailed description of the mechanism can be found e.g. in [78, 80]. As mentioned above, enclosed air bubbles are exposed to over-pressure which is inversely proportional to the bubble radius. In

addition, the air solubility is proportional to the over-pressure. Thus, the smaller the pore, the faster the dissolution of air and water filling of the pore. Fagerlund [80] proposed two models for water-filling of air bubbles: Model 1 where absorption takes place in bubbles of all sizes simultaneously, and Model 2, where small bubbles are saturated before absorption in larger bubbles is initiated. According to Fagerlund [80], Model 2 is most plausible from a thermodynamic point of view. Assuming, among others, an air bubble surrounded by saturated paste and a large number of very big pores at a distance 5 times the radius of the air bubble, Fagerlund [78] calculated the time for water-filling of air bubbles of different sizes. The impact of the pore size and the assumed diffusivity of dissolved air on the estimated time needed for water-filling is illustrated in Fig. 10. The absorption time needed to fill a pore is longer for coarse pores and for materials with low permeability. Data for the impact of *w/c* and binder type on air diffusivity can be found in e.g. [81].

Temperature cycles and freeze/thaw cycles are observed to increase the sorptivity of concrete [82, 83]. It is also likely that the rate of filling of air voids will be affected; but no such information seems to be available in the literature.

The work of Jacobsen et al. [84] indicated that air voids might become water filled in the absence of hydrostatic pressure. Investigating the effect of pre-conditioning on frost resistance and ascribing

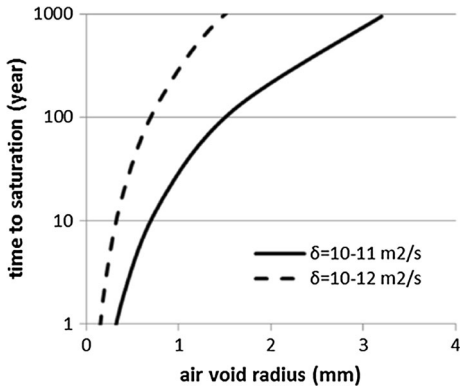

Fig. 10 Estimated time to water-filling of air voids by dissolution of air [77]. ($t = 9.0 \times 10^6 \times r^3/\delta$; t: time (s); r: air void radius (m); δ: air diffusivity in water (m^2/s). Assumptions: $\delta = 10^{-11}$ m^2/s or $\delta = 10^{-12}$ m^2/s ($\delta = 2 \times 10^{-9}$ in bulk water if concentration in kg/m^3); solubility of air in water, $s = 2.5 \times 10^{-7}$ $kg/(m^3$ Pa); spacing between bubbles is supposed to be 5 times the air-pore radius; density of air at atmospheric pressure, $\rho = 1.2$ kg/m^3)

absorption during wet curing in excess of theoretical self-desiccation to water filling of voids, they calculated that significant parts of the air voids became water filled during saturated curing. For the investigated concretes, the degree of saturation of air voids was 10–65% after water curing for 80 days (cylinders ø100 × 200 or ø150 × 300 mm, $w/b = 0.45$, approx. 350 kg/m^3 Portland cement, with and without 5% silica fume, 3–6% air voids of concrete volume).

Hedenblad et al. [85] and De Weerdt et al. [86] provided data for moisture content in marine concrete submerged for 14 and 16 years, respectively. Both found the degree of capillary saturation (S_{cap}) of bulk concrete in the range of 90–95%. The concrete compositions varied from $w/b = 0.38$ and a few percent of silica fume to w/b in the range of 0.40–0.44 and binders containing Portland cement and silica fume, fly ash or slag. Higher capillary saturation was found near the surface, up to 98% in the outer 10 mm [86]. The absence of full capillary saturation indicates that no air-pores are water-filled [87]. According to theory, dissolution of air requires the establishment of an over-pressure, which requires capillary saturation of the matrix [77]. In contrast to the observations on approximately 15 years old submerged marine concrete, Rosenqvist [88] found capillary saturated conditions in a concrete dam ($w/c = 0.55$) exposed to fresh water for 55 years. The concrete at levels 0 and −18.5 m was capillary saturated to a depth of 20 mm and 200 mm, respectively.

The moisture state in Norwegian coastal bridges was investigated by Relling [89, 90]. Selected data were published in [89]. Table 2 provides an overview of measured degree of capillary saturation (S_{cap}) observed in the outer 40–50 mm of the concrete. It can be observed that the degree of saturation is high in structural elements exposed to the tidal zone, but not in the columns and superstructure. In addition to the impact of exposure, orientation dependent variations in degree of saturation were observed on the same structure. Furthermore, Relling [90] found that chloride contamination affected the sorption isotherm; a higher moisture content—and thus degree of saturation—was found in chloride contaminated concrete.

Concrete cores from 26 Danish structures of varying age (built 1953–1985) were investigated in a 1996 project on freeze/thaw performance testing [91]. The investigation included Portland cement concretes

Table 2 Overview of average moisture content (degree of capillary saturation, S_{cap}) from first 40 or 50 mm in 11 Norwegian costal bridges and the inland 'Smedstua' and in near surface and internal concrete in 26 Danish concrete structures

Structural element/exposure	Depth	Number	S_{cap}	CV	Ref.
Superstructures (marine)	0–40/50 mm	70	81.9	6.7	[89]
Columns (marine)	0–40/50 mm	114	81.6	6.9	
Tidal zone (marine)	0–40/50 mm	45	96.6	2.9	
Smedstua, super structure and abutment (inland)	0–40/50 mm	16	76.0	4.6	
Exposure to frost and water, with or without salt	'Surface near'	14	83	14	[91]
	'Internal'	14	92	6	
Exposure to frost and sometimes water, with or without salt	'Surface near'	7	79	8	
	'Internal'	7	88	5	
Vertical surfaces exposed to frost, but rarely to water and not to salt	'Surface near'	5	75	7	
	'Internal'	5	84	3	

CV coefficient of variation

(*w/c* generally 0.35–0.45) with and without fly ash and silica fume. The degree of capillary saturation is given in Table 2. It can be observed that several of the investigated concrete elements had a high degree of saturation; especially internally. A few of the concretes were close to or at capillary saturation. All concrete contained empty voids, which only were water filled upon pressure saturation.

In summary, macroscopic voids in concrete are commonly not saturated under exposure conditions expected in situ. Very few of the investigated in situ exposed structures were fully capillary saturated. It may thus be anticipated that only an adsorbed water film will cover the pore walls of macroscopic void under in situ exposure conditions. However, theoretical studies, experimental investigations under laboratory conditions, and investigations of a 55 year old concrete dam show that air voids might become filled. The proposed mechanism is that dissolution of the entrapped air into the surrounding pore water leads to a gradual filling of the pore with liquid water in the over-capillary range. In addition to water filling, air voids might be (partly) filled by re-precipitated hydrates, typically ettringite.

As mentioned in Sect. 2.4, the microstructure of the concrete part of the SCI is similar to the ITZ around aggregates, but different from bulk concrete. Essentially, the capillary porosity at the SCI will be higher than in the bulk concrete further away. This will affect the sorption isotherm and thus the degree of saturation at a given RH as well as the rate of diffusion of air. Furthermore, possible temperature differences between steel and concrete might create non-equilibrium moisture conditions, e.g. cooling of the steel could lead to condensation at the steel surface.

2.5.5 *Filling of macroscopic pores with solids*

According to Samson et al. [92] precipitation of ettringite is thermodynamically possible in voids and it is not limited to (partially) saturated conditions. This is supported by microscopic observations by Jakobsen [93]. Based on simple calculations indicating that max 2% ettringite of the total volume of concrete can be formed from the amount of sulfate in a typical concrete, Samson et al. [92] concluded that air void filling should not be a problem with regard to freeze/thaw damage in properly air-entrained concrete. However, accumulation of sulfate due to zoning or ingress might increase the amount in some areas. This is illustrated by data from a 55 years old Swedish concrete dam ($w/c = 0.55$) exposed to fresh water, where extensive filling of air voids by ettringite was found a surface near zone (approx. 3–8 mm) [94].

2.6 Miscellaneous possible characteristics at the SCI

2.6.1 *Neighbouring or intersecting rebars and tie wires*

It is well known that dense detailing of reinforcing steel can lead to incomplete compaction and locally porous or segregated concrete [95]. While this is an

extreme case representing bad construction practice, intersecting rebars and the presence of tie wires frequently occur in standard engineering structures (but generally not in laboratory samples). Figure 11 shows a section through a crossing-point of two perpendicular rebars with macroscopic voids formed between the bars.

In a laboratory investigation, concrete slabs (1 m × 1 m × 0.1 m, Portland cement, $w/c = 0.55$, admixed chloride: 5% by wt. of cement) with perpendicularly intersecting rebars (∅10 mm, polished and degreased) were cast, and cured under sprinkling water for 28 days [96]. Besides corrosion measurements, concrete samples were taken from the location of intersecting rebars and far from intersections (by breaking the specimens) and analysed by means of scanning electron microscopy (SEM) and mercury intrusion porosimetry (MIP). The concrete at the SCI far from the rebar intersections was found to be significantly less porous than the concrete at the SCI close to the intersection of two rebars. The results may, however, have been affected by the presence of corrosion products that lead to cracking of the concrete, particularly at rebar intersections.

Tie wires introduce a comparable geometrical restriction to the flow and compaction of concrete at the SCI as rebar intersections. In case of welded rebar mats, apart from geometrical peculiarities the areas affected by the welding heat may undergo metallurgical transformations and show different electrochemical behaviour (thus corrosion resistance) [97].

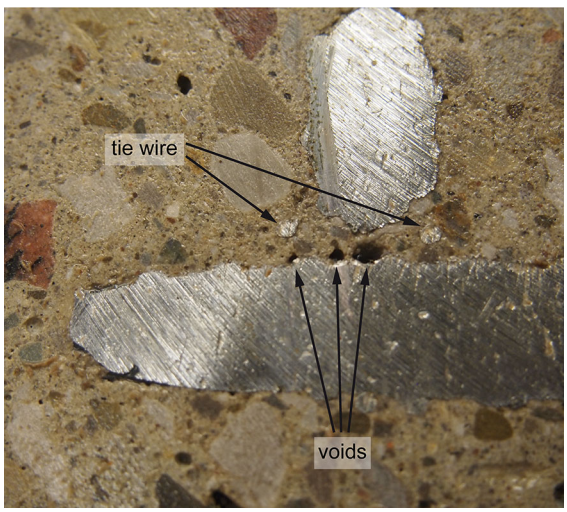

Fig. 11 Example of voids formed at the intersection of perpendicular rebars (photograph courtesy of Colin Van Niejenuis, University of Waterloo, Canada)

2.6.2 *Presence of spacers in the concrete cover*

Spacers are essential components in reinforced concrete structures. Spacers (i.e. bar supports, wire chairs, bolsters, etc.) are used to secure steel reinforcements within the formwork to prevent movement prior to and during concreting so that the required cover is obtained in the finished structure. Spacers are made of plastic, metal or cementitious materials, and are available in various sizes and shapes [98–100]. They generally fall into one of six categories: (a) plastic spacers with integral clip-on action for horizontal rebars of 20 mm diameter or less, (b) plastic end spacers for end cover, (c) plastic wheel/circular spacers for vertical rebars, (d) cementitious block spacers for bar size > 20 mm in heavily-reinforced sections; (e) continuous line spacers of constant cross-section to support several bars; and f) steel wire chairs that may be single, continuous or circular, to support the top horizontal rebar from lower rebar or to separate layers of vertical rebars.

There are a number of standards containing specifications for spacers and for their placement, e.g. [101–103]. The general rule is that spacers should be fixed to reinforcing bars at a spacing not exceeding 50 x ∅ or 1000 mm, where ∅ is the rebar diameter, and in staggered rows for parallel bars.

Similar to intersecting/neighbouring rebars (cf. Sect. 2.6.1) the presence of spacers as solid material in contact or close proximity of the steel surface likely affects the local concrete microstructure and gives rise to crevices at the SCI. While the effect of spacers on the concrete cover have been studied [104], documentation of the properties at the SCI is largely lacking. Figure 12 shows an example of the contact zone between a spacer and the reinforcing steel bar.

2.6.3 *Presence of metallic or plastic ducts*

In post-tensioned structures, to ensure the positioning of the tendons, the duct has to be tied to the reinforcing steel cage, preferably at duct support bars. Depending on the curvature of the tendon the spacing of duct support bars may vary greatly. Occasionally, ducts may also be fixed to stirrups, but this is not considered

Fig. 12 Sectioned concrete showing an example of a plastic contact spacer as inherent part of concrete and reinforcing steel bars (photograph courtesy of Hong Wong, Imperial College, London, UK)

good construction practice [105]. Also at points where the duct is not tied to the reinforcing steel, it may be in physical contact with rebars [106]. In any case, the immediate proximity of reinforcing steel and ducts—either metallic or plastic—is likely to affect the concrete microstructure at the SCI. To our knowledge, there is no systematic documentation of this.

One may argue that the cover depth of tendons is usually significantly larger than that of the reinforcing steel layers closest to the concrete surface, and thus these local inhomogeneities at the SCI may generally not be found at the most severely exposed layer of reinforcing steel. Nevertheless, despite the specifications of modern construction standards, experience from existing engineering structures has shown that tendons may be located at shallow cover depths [106, 107].

2.6.4 Contamination of steel surface

During the construction process on-site, various substances are unintentionally deposited on the reinforcing steel surface prior to casting [108, 109]. These include form oil, concrete splatter, dirt, etc. While international construction standards generally state that the reinforcing steel must be free from any surface contaminants, it is known that in practice this desirable state may not always be fully achieved. Several studies concluded that these surface contaminants generally have little influence on mechanical bond between ribbed/indented rebars and concrete [108–110], but there is little documentation on the effect on other properties of the SCI (e.g. microstructure, cement hydration phases and metal oxides/hydroxides present, etc.).

Concerning concrete splatter, depending on exposure duration and conditions (e.g. dry, warm climate), these deposited cement paste or mortar layers may be cracked due to drying shrinkage and/or carbonated by the time concrete is cast. Obviously, this introduces another local inhomogeneity at the SCI; systematic investigations are however lacking.

2.6.5 Concrete inhomogeneities related to flow direction during concrete placement

Occasionally, it has been observed that the flow direction during concrete placement may lead to concrete inhomogeneities on the far side (with respect to flow direction) of reinforcing steel bars. Typically, there will be a decrease in content of coarse aggregates behind a rebar; in some cases, even voids may form.

3 Discussion

3.1 Occurrence in the laboratory and in reality

3.1.1 Laboratory specimens versus engineering structures

The columns entitled “lab” and “on-site” in Table 1 indicate whether the different local characteristics can be found primarily in laboratory specimens or in engineering structures, or in both situations. Needless to say, laboratory conditions should in general mimic reality. Typical features that are frequently present in concrete structures, but rarely in laboratory samples are for instance intersections of rebars, tie wires, spacers, or contaminated rebar surface. Additionally, the surfaces of reinforcing steel used in laboratory studies are often different to those used in real structures. An evaluation [2] of more than 50 publications describing corrosion tests in concrete revealed that in a large part of the studies (41%) the rebar surface condition was not considered important (no details about mill scale or pre-existing rust layers reported); while some authors reported that the rebar

surface was sandblasted (12%), polished (32%), or left in as-received condition (14%).

Regarding the concrete, it is well known that laboratory investigations—due to their relatively small specimen dimensions—often use mortar instead of concrete, which strongly affects the size of aggregates at the SCI. Furthermore, the procedures for placing, compacting, and curing concrete, which may affect the concrete microstructure at the SCI, are different in laboratory studies compared with construction site practice.

Other major differences between laboratory specimens and engineering structures are the age and exposure conditions. While laboratory samples are generally young (from a few days or months to at best a few years) and kept in controlled environment, engineering structures exhibit service lives in the order of decades and are subjected to varying environmental and mechanical loads. Concerning air voids in the matrix, on the other hand, there seem not to be large differences between laboratory specimens and engineering structures (only one study [68] available). Little is, however, known regarding the degree of water filling of these voids.

3.1.2 Differences among engineering structures and structural members

Engineering structures around the world may exhibit marked differences due to differences in national/local construction policies, building codes, and workmanship as well as climatic exposure conditions.

One of the most important factors giving rise to differences among engineering structures is the type of concrete used. Over the last century, concrete technology has undergone major transformations, such as the advent of concrete admixtures, particularly superplasticizers that made it possible to produce concrete with extremely low water/binder ratios. In conjunction with the increasing use of supplementary cementitious materials this led to modern concretes that can hardly be compared to traditional concrete in terms of many properties such as pore structure, pore solution chemistry, etc. (see Sect. 2.4).

Although steel is generally considered a much more homogeneous material than concrete—particularly concerning mechanical material parameters—it has been shown in Sect. 2.2 that reinforcing steel for concrete may be very different in terms of bar geometry (ribbed, indented, twisted, etc. bars), chemical composition and steel microstructure. In contrast to concrete, however, codes, standards, and owner policies exercise much less control over the chemical composition and microstructure of reinforcing steel. Typically, standards impose requirements regarding mechanical properties, geometrical specifications, and properties such as weldability or ductility. Thus, as long as reinforcing steel satisfies these criteria, it may still exhibit considerable differences in terms of chemical composition and microstructure, depending on origin and manufacturer [19].

Similar to concrete, technological evolution over time has strongly impacted reinforcing steel as discussed in Sect. 2.2. Concerning rebar geometry, for instance, up to ca. 1925, primarily steel of round or square cross section was used [13]. Later on, to improve bond and anchorage, a wide variety of irregular (rather than smooth) rebar surface geometries were marketed, including cold twisted square bars, and various corrugated and deformed bars. Today, European standard EN 10800, for instance, distinguishes between "ribbed steel" and "indented steel" and stipulates tolerances for the dimensions and number of ribs and indentations, respectively [14]. The geometry of the reinforcing steel (location of ribs) has an influence on the SCI, e.g. by causing local bleed water zones under ribs or between indentations and by defining the location of cracking (see Sect. 2.5). Additionally, in the 1970/80 s, a transition from cold-work hardening to thermomechanically strengthened steels occurred (Sect. 2.2), which strongly influences the steel microstructure and surface condition.

Finally, also the type of engineering structure (e.g. bridge, tunnel, retaining wall, etc.) and its structural members (slab, beam, column, wall, etc.) will influence the SCI due to differences in geometry, construction process, exposure, and mechanical stresses.

In summary, considering the progress in concrete technology and in reinforcing steel manufacturing, young (ca. $<$ 20–30 years) and future structures are likely to have significantly different SCIs than older structures. Unfortunately, all long-term field experience on the durability performance of reinforced concrete essentially stems from the latter; given the described significant differences in SCI properties, this accumulated knowledge may not be applicable to young and future structures may not be given.

3.2 Interrelations

Figure 13 schematically details possible interrelations between different characteristics of the SCI. For example, the geometry of the reinforcing steel bars, i.e. their diameter and rib shape, their orientation in the concrete (e.g. vertical or horizontal), will affect the presence or absence of voids such as bleed water zones or entrapped air voids in the concrete. To give another example, the local concrete microstructure and the phases present impact the composition and amount of electrolyte in the concrete pore system, which in turn influences transformations in native rust layers on the steel surface and the formation and properties of the passive film on the steel surface.

The figure illustrates that there are numerous mutual influences between the different characteristics related to the steel and the concrete. Thus, even when using an "identical" concrete mix, the SCI will be different depending on the type of reinforcing steel, geometrical factors (e.g. casting direction) and also on later exposure (discussed in the next section).

3.3 Influences of exposure and time

Many characteristics of the SCI are influenced by environmental exposure and by structural loads (Fig. 13). Structures are differently exposed to moisture (different relative humidities, direct sunlight, direct exposure to splash water, or immersed in water) and often this is also changing over time, e.g. due to seasonal variations. The same is true for the exposure temperature. Additionally, chemical exposure may differ strongly (chlorides, carbon dioxide concentration, sulfates, etc.). Figure 13 shows how these may eventually affect the SCI. It is important to recognize, however, that the cover concrete typically shields the SCI from environmental exposures, at least for a certain time. Exceptions are locations with cracks, honeycombs and other areas where the SCI has direct access to the exposure environment.

Mechanical stresses may arise from structural loads as well as from volume changes caused by environmental exposures, such as moisture and/or temperature changes or chemical exposure (Fig. 13). Mechanical stresses primarily cause cracking, slip, and delamination at the SCI, but they may also affect the morphology of the passive layer and of other iron oxides/hydroxides on the steel surface.

Finally, there are a number of characteristics at the SCI that change over time, even at constant exposure conditions because of the slow kinetics of the underlying processes. Examples are concrete microstructure (cement hydration, self-desiccation), passive layer growth, or transformations in native rust layers or mill-scales. These time-dependent changes at the SCI may be understood as "ageing processes", occurring over long time spans.

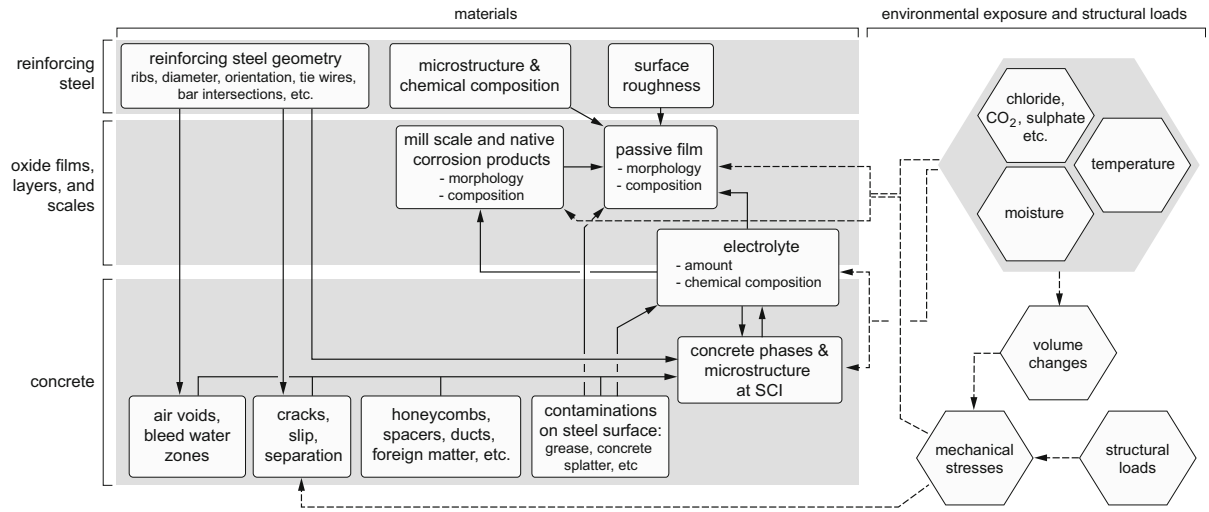

Fig. 13 Schematic illustration of interrelations between different characteristics at the SCI and of influences by environmental exposure (temperature, moisture, and chemical exposure) and structural loads

4 Conclusions

We made a comprehensive list of possible local characteristics at the steel–concrete interface (SCI) and compiled available information regarding their properties as well as the occurrence of these characteristics in laboratory and in engineering structures. Given the complexity of the SCI, we suggested a systematic approach to describe it in terms of local characteristics (Fig. 2; Table 1). We also described possible interrelations between these (Fig. 13).

The following major conclusions are drawn:

- The SCI exhibits significant spatial inhomogeneity along and around as well as perpendicular to the reinforcing steel bar in terms of material composition and physical and chemical properties. The different features that can be found at the SCI span over a large range of dimensions, i.e. from the nanometer scale (e.g. passive layer) to the order of centimeters or even decimeters (e.g. voids or honeycombs).
- The SCI properties continuously change as a function of time-dependent exposure conditions, structural loading, and material ageing (cement hydration, passive layer growth, etc.).
- The SCI can differ strongly between different engineering structures and also between different members within a structure, since some of the characteristics listed in Table 1 may be present or absent in different cases. Particular differences are expected between structures built before and after the 1970/80 s due to the developments in concrete technology and in reinforcing steel manufacturing processes. A single SCI representing all on-site conditions does not exist.
- SCIs in laboratory-made specimens frequently exhibit significant differences compared to those in engineering structures. For instance, any steel surface cleaning procedures removing mill scale, native rust layers or affecting surface roughness in the laboratory is expected to lead to conditions at the SCI not representative of engineering structures. Other deviations from engineering structures that we consider relevant are the common laboratory practice of extended curing regime, the absence of cracks and other mechanical damage in unloaded laboratory specimens, the possible differences in concrete microstructure, the frequent absence of rebar intersections, tie wires, spacers, or welding points, and finally the lack of long ageing times and realistic exposure.
- In the literature, there is documentation for the physical and chemical properties as well as the frequency of occurrence of the following characteristics: macroscopic voids at the SCI, concrete microstructure, rebar geometry, and rebar microstructure. On the other hand, there is a lack of documentation concerning the following: moisture conditions in voids at the SCI, steel surface conditions, and characteristics such as rebar intersections, tie wires, welding points, and contaminations.
- The SCI is known to affect the durability performance of reinforced concrete structures. In this work, large differences of SCI properties were identified between laboratory samples and engineering structures. Thus, results from laboratory studies should be applied to engineering structures with caution. Furthermore, there may be significant differences between different engineering structures (e.g. concerning the time of construction, construction practices, etc.) and thus, practical experience from one structure may not be directly applicable to other structures.

Based on these conclusions, we suggest to use the systematic approach to the SCI proposed in this work as a basis to identify from the comprehensive list in Table 1 those characteristics that have the most dominant effect on the durability (corrosion) of reinforced concrete. This will lay the basis for further research to study the influence of SCI characteristics on durability in detail. A better understanding of the SCI and its role in corrosion of steel in concrete are essential to improve engineering models for the prediction of the corrosion performance of concrete structures.

Acknowledgements The authors thank Joost Gulikers for his comments and careful reading of the manuscript.

Compliance with ethical standards

Conflict of interest The authors declare that they have no conflict of interest.

Open Access This article is distributed under the terms of the Creative Commons Attribution 4.0 International License (http://creativecommons.org/licenses/by/4.0/), which permits unrestricted use, distribution, and reproduction in any medium, provided you give appropriate credit to the original

author(s) and the source, provide a link to the Creative Commons license, and indicate if changes were made.

References

1. Angst UM, Elsener E (in press) Chloride threshold values in concrete—a look back and ahead. ACI Special Publication "Chloride Limits and Thresholds for Concrete Containing Supplementary Cementitious Materials (SCM's)"
2. Angst U, Elsener B, Larsen CK, Vennesland Ø (2009) Critical chloride content in reinforced concrete—a review. Cem Concr Res 39(12):1122–1138
3. Reddy B (2001) Influence of the steel–concrete interface on the chloride threshold level. PhD thesis, Imperial College, London
4. Buenfeld NR, Glass GK, Reddy B, Viles RF (2004) Process for the protection of reinforcement in reinforced concrete. US Patent 6,685,822 B2
5. Glass GK, Reddy B (2002) The influence of the steel concrete interface on the risk of chloride induced corrosion initiation. In: COST 521: Final Single Project Reports, UK6Brussels, pp 227–232
6. Castel A, Vidal T, Francois R, Arliguie G (2003) Influence of steel–concrete interface quality on reinforcement corrosion induced by chlorides. Mag Concr Res 55(2):151–159
7. Soylev TA, Francois R (2003) Quality of steel–concrete interface and corrosion of reinforcing steel. Cem Concr Res 33(9):1407–1415
8. Harnisch J, Raupach M (2011) Untersuchungen zum kritischen korrosionsauslösenden Chloridgehalt unter Berücksichtigung der Kontaktzone zwischen Stahl und Beton. Beton- Und Stahlbetonbau 106(5):299–307
9. Angst U (2011) Chloride induced reinforcement corrosion in concrete; concept of critical chloride content—methods and mechanisms. PhD thesis, Norwegian University of Science and Technology, NTNU, Trondheim
10. Michel A, Solgaard AOS, Pease BJ, Geiker MR, Stang H, Olesen JF (2013) Experimental investigation of the relation between damage at the concrete–steel interface and initiation of reinforcement corrosion in plain and fibre reinforced concrete. Corros Sci 77:308–321
11. Mohammed TU, Otsuki N, Hamada H (2003) Corrosion of steel bars in cracked concrete under marine environment. J Mater Civil Eng 15(5):460–469
12. Wayne R (2014) Light and video microscopy. Academic Press, San Diego
13. Bindseil P, Schmitt MOA (2002) Betonstähle (in German). Verlag Bauwesen, Berlin
14. European Committee for Standardization (2005) EN 10080:2005—Steel for the reinforcement of concrete. Weldable reinforcing steel. General
15. Rehm G, Russwurm D (1977) Assessment of concrete reinforcing bars by the Tempcore process. Betonwek + Fertigteil-Technik 6:300–307
16. Ray A, Mukerjee D, Sen SK, Bhattacharya A, Dhua SK, Prasad MS, Banerjee N, Popli AM, Sahu AK (1997) Microstructure and properties of thermomechanically strengthened reinforcement bars: a comparative assessment of plain-carbon and low-alloy steel grades. J Mater Eng Perform 6(3):335–343
17. Nikolaou J, Papadimitriou GD (2004) Microstructures and mechanical properties afteir heating of reinforcing 500 MPa class weldable steels produced by various processes (Tempcore, microalloyed with vanadium and workhardened). Constr Build Mater 18(4):243–254
18. Cadoni E, Dotta M, Forni D, Tesio N, Albertini C (2013) Mechanical behaviour of quenched and self-tempered reinforcing steel in tension under high strain rate. Mater Des 49:657–666
19. Angst UM, Elsener B (2015) Forecasting chloride-induced reinforcement corrosion in concrete—effect of realistic reinforcement steel surface conditions. In: Proceedings of 4th international conference on concrete repair, rehabilitation and retrofitting (ICCRRR), Leipzig
20. Okamoto A, Nakamura H (1990) The influence of residual-stress on fatigue cracking. J Press Vessel Technol Trans ASME 112(3):199–203
21. Zheng H, Abel AA (1999) Fatigue properties of reinforcing steel produced by TEMPCORE process. J Mater Civil Eng 11(2):158–165
22. Raman RKS (2006) Characterisation of 'rolled-in', 'fragmented' and 'red' scale formation during secondary processing of steels. Eng Fail Anal 13(7):1044–1050
23. Ghods P, Isgor OB, McRae GA, Li J, Gu GP (2011) Microscopic investigation of mill scale and its proposed effect on the variability of chloride-induced depassivation of carbon steel rebar. Corros Sci 53(3):946–954
24. Trejo D, Monteiro PJ (2005) Corrosion performance of conventional (ASTM A615) and low-alloy (ASTM A706) reinforcing bars embedded in concrete and exposed to chloride environments. Cem Concr Res 35(3):562–571
25. Wong HS, Zhao YX, Karimi AR, Buenfeld NR, Jin WL (2010) On the penetration of corrosion products from reinforcing steel into concrete due to chloride-induced corrosion. Corros Sci 52(7):2469–2480
26. Poursaee A, Hansson CM (2007) Reinforcing steel passivation in mortar and pore solution. Cem Concr Res 37(7):1127–1133
27. Demoulin A, Trigance C, Neff D, Foy E, Dillmann P, L'Hostis V (2010) The evolution of the corrosion of iron in hydraulic binders analysed from 46- and 260-year-old buildings. Corros Sci 52(10):3168–3179
28. Walsh MT, Sagüés AA (2016) Steel corrosion in submerged concrete structures—Part 1: field observations and corrosion distribution modeling. Corrosion 72:518–533
29. Stefanoni M, Angst U, Elsener B (2015) Local electrochemistry of reinforcement steel—distribution of open circuit and pitting potentials on steels with different surface condition. Corros Sci 98:610–618
30. Ghods P, Isgor OB, Mcrae GA, Cu GP (2010) Electrochemical investigation of chloride-induced depassivation of black steel rebar under simulated service conditions. Corros Sci 52(5):1649–1659
31. El Haleem SMA, El Wanees SA, El Aal EEA, Diab A (2010) Environmental factors affecting the corrosion behavior of reinforcing steel II. Role of some anions in the initiation and inhibition of pitting corrosion of steel in Ca(OH)(2) solutions. Corros Sci 52(2):292–302

32. Li L, Sagüés AA (2001) Chloride corrosion threshold of reinforcing steel in alkaline solutions—open-circuit immersion tests. Corrosion 57(1):19–28
33. Flis J, Pickering HW, Osseo-Asare K (1998) Interpretation of impedance data for reinforcing steel in alkaline solution containing chlorides and acetates. Electrochim Acta 43(12–13):1921–1929
34. Rossi A, Puddu G, Elsener B (2007) The surface of iron and Fe10Cr in alkaline media. In: Raupach M, Elsener B, Polder R, Mietz J (eds) Corrosion of reinforcement in concrete—mechanisms, monitoring, inhibitors and rehabilitation techniques, EFC Publication no. 3844-60
35. Feng LJ, Yang HY, Wang FH (2011) Experimental and theoretical studies for corrosion inhibition of carbon steel by imidazoline derivative in 5% NaCl saturated Ca(OH)(2) solution. Electrochim Acta 58:427–436
36. Chen YM, Orazem ME (2016) Impedance analysis of ASTM A416 tendon steel corrosion in alkaline simulated pore solutions. Corros Sci 104:26–35
37. Sanchez M, Gregori J, Alonso C, Garcia-Jareno JJ, Takenouti H, Vicente F (2007) Electrochemical impedance spectroscopy for studying passive layers on steel rebars immersed in alkaline solutions simulating concrete pores. Electrochim Acta 52(27):7634–7641
38. Volpi E, Olietti A, Stefanoni M, Trasatti SP (2015) Electrochemical characterization of mild steel in alkaline solutions simulating concrete environment. J Electroanal Chem 736:38–46
39. Williamson J, Isgor OB (2016) The effect of simulated concrete pore solution composition and chlorides on the electronic properties of passive films on carbon steel rebar. Corros Sci 106:82–95
40. Poursaee A (2010) Corrosion of steel bars in saturated Ca(OH)2 and concrete pore solution. Concr Res Lett 1:90–97
41. Ghods P, Isgor OB, Mcrae G, Miller T (2009) The effect of concrete pore solution composition on the quality of passive oxide films on black steel reinforcement. Cem Concr Compos 31(1):2–11
42. Hansson CM, Poursaee A, Laurent A (2006) Macrocell and microcell corrosion of steel in ordinary Portland cement and high performance concretes. Cem Concr Res 36(11):2098–2102
43. Haupt S, Strehblow HH (1987) Corrosion, layer formation, and oxide reduction of passive iron in alkaline-solution—a combined electrochemical and surface analytical study. Langmuir 3(6):873–885
44. Ghods P, Isgor OB, Brown JR, Bensebaa F, Kingston D (2011) XPS depth profiling study on the passive oxide film of carbon steel in saturated calcium hydroxide solution and the effect of chloride on the film properties. Appl Surf Sci 257(10):4669–4677
45. Andrade C, Merino P, Novoa XR, Perez MC, Solar L (1995) Passivation of reinforcing steel in concrete. Mater Sci Forum 861:192–194
46. Ghods P, Isgor OB, Carpenter GJC, Li J, McRae GA, Gu GP (2013) Nano-scale study of passive films and chloride-induced depassivation of carbon steel rebar in simulated concrete pore solutions using FIB/TEM. Cem Concr Res 47:55–68
47. Gunay HB, Ghods P, Isgor OB, Carpenter GJC, Wu XH (2013) Characterization of atomic structure of oxide films on carbon steel in simulated concrete pore solutions using EELS. Appl Surf Sci 274:195–202
48. Feng XG, Zuo Y, Tang YM, Zhao XH, Lu XY (2011) The degradation of passive film on carbon steel in concrete pore solution under compressive and tensile stresses. Electrochim Acta 58:258–263
49. Feng XG, Tang YM, Zuo Y (2011) Influence of stress on passive behaviour of steel bars in concrete pore solution. Corros Sci 53(4):1304–1311
50. Mammoliti LT, Brown LC, Hansson CM, Hope BB (1996) The influence of surface finish of reinforcing steel and pH of the test solution on the chloride threshold concentration for corrosion initiation in synthetic pore solutions. Cem Concr Res 26(4):545–550
51. Bensabra H, Azzouz N (2013) Study of rust effect on the corrosion behavior of reinforcement steel using impedance spectroscopy. Metall Mater Trans A 44a(13):5703–5710
52. Mohammed TU, Hamada H (2006) Corrosion of steel bars in concrete with various steel surface conditions. ACI Mater J 103(4):233–242
53. Akhoondan M, Sagüés A (2012) Comparative cathodic behavior of $\sim$ 9% Cr and plain steel reinforcement in concrete. Corrosion 68:1–10
54. Li L, Sagüés AA (2004) Chloride corrosion threshold of reinforcing steel in alkaline solutions—effect of specimen size. Corrosion 60(2):195–202
55. Angst U, Rønnquist A, Elsener B, Larsen CK, Vennesland Ø (2011) Probabilistic considerations on the effect of specimen size on the critical chloride content in reinforced concrete. Corros Sci 53(1):177–187
56. Scrivener KL, Crumbie AK, Laugesen P (2004) The interfacial transition zone (ITZ) between cement paste and aggregate in concrete. Interface Sci 12(4):411–421
57. Horne AT, Richardson IG, Brydson RMD (2007) Quantitative analysis of the microstructure of interfaces in steel reinforced concrete. Cem Concr Res 37(12):1613–1623
58. Bäumel A (1959) Die Auswirkung von Betonzusatzmitteln auf das Korrosionsverhalten von Stahl in Beton (in German). Zement-Kalk-Gips 7:294–305
59. Page CL (1975) Mechanism of corrosion protection in reinforced concrete marine structures. Nature 258:514–515
60. Page CL (2009) Initiation of chloride-induced corrosion of steel in concrete: role of the interfacial zone. Mater Corros 60(8):586–592
61. Glass GK, Yang R, Dickhaus T, Buenfeld NR (2001) Backstatered electron imaging of the steel–concrete interface. Corros Sci 43:605–610
62. Gjorv OE, Monteiro PJM, Mehta PK (1990) Effect of condensed silica fume on the steel–concrete bond. ACI Mater J 87(6):573–580
63. Larbi JA (1993) Microstructure of the interfacial zone around aggregate particles in concrete. Heron 38(1):5–69
64. Vollpracht A, Lothenbach B, Snellings R, Haufe J (2016) The pore solution of blended cements: a review. Mater Struct 49(8):3341–3367
65. Jakobsen UH, Weerdt KD, Geiker MR (2016) Elemental zonation in marine concrete. Cem Concr Res 85:12–27
66. Mielenz RC, Wolkodoff VE, Backstrom JE, Flack HL (1958) Orgin, evolution, and effects of the air void system in concrete. Part 1—etrained air in unhardend concrete. Proc Am Concr Inst 55(7):95–121

67. Richardson M (2007) Degradation of concrete in cold weather conditions. In: Page CL, Page MM (eds) Durability of concrete and cement composites. Woodhead Publishing Limited, Cambridge, pp 282–315
68. Mielenz RC, Wolkodoff VE, Backstrom JE, Burrows RW (1958) Orgin, evolution, and effects of the air void system in concrete. Part 4—the air void system in job concrete. Proc Am Concr Inst 55(10):507–517
69. Castel A, Vidal T, Viriyametanont K, Francois R (2006) Effect of reinforcing bar orientation and location on bond with self-consolidating concrete. Aci Struct J 103(4):559–567
70. Zhang RJ, Castel A, Francois R (2011) Influence of steel–concrete interface defects owing to the top-bar effect on the chloride-induced corrosion of reinforcement. Mag Concrete Res 63(10):773–781
71. Mohammed TU, Otsuki N, Hamada H, Yamaji T (2002) Chloride-induced corrosion of steel bars in concrete with presence of gap at steel–concrete interface. ACI Mater J 99(2):149–156
72. Goto Y (1971) Cracks formed in concrete around deformed tension bars. J Am Concr Inst 68:244–251
73. Tammo K, Lundgren K, Thelandersson S (2009) Nonlinear analysis of crack widths in reinforced concrete. Mag Concr Res 61(1):23–34
74. ACI Committee 224 (2001) Cracking of concrete members in direct tension. American Concrete Institute, Farmington Hills
75. Comité Euro-Internationale du Béton (1985) Design Manual on Cracking and Deformations. École Polytechnique Fédérale de Lausanne, Switzerland
76. Borosnyói A, Balázs GL (2005) Models for flexural cracking in concrete: the state of the art. Struct Concr 6:53–62
77. Fagerlund G (2006) Moisture design with regards to durability—with special reference to frost destruction. Report TVBM-3130. Lund University, Sweden
78. Fagerlund G (2004) A service life model for internal frost damage in concrete. Report TVBM-3119. Lund institute of Technology, Sweden
79. Mehta PK, Monteiro PJM (2006) Concrete microstructure, properties, and materials. McGraw-Hill, New York
80. Fagerlund G (1993) The long time water absorption in the air-pore structure of concrete. Report TVBM-3051
81. Fagerlund G (1982) The influence of slag content on frost resistance of hardened concrete
82. Geiker MR, Laugesen P (2001) On the effect of laboratory conditioning and freeze/thaw exposure on moisture profiles in HPC. Cem Concr Res 31(12):1831–1836
83. Wikiström T (2012) Vattenabsorption i betong under inverkan av temperatur. Report TVBM-5084
84. Jacobsen S, Marchand J, Boisvert L, Pigeon M, Sellevold EJ (1997) Frost deicer salt scaling testing of concrete: effect of drying and natural weathering. Cem Concr Aggr 19(1):8–16
85. Hedenblad G, Andersen A, Nilsson L-O (1998) Fältmätningar i utomhuskonstruktioner (in Swedish). M8:8. Byggnadsmaterial. Lunds Tekniska Högskola, Sweden
86. De Weerdt K, Orsakova D, Müller A, Larsen CK, Pedersen B, Geiker M (2016) Towards the understanding of chloride profiles in marine exposed concrete, impact of leaching and moisture content. Constr Build Mater 120(1):418–431
87. Fagerlund G (1993) Frostangrepp – beskrivning av verkande mekanismer. Marina betong-konstruksjoners livsläng. Cementa AB, Danderyd
88. Rosenqvist M (2016) Frost-induced deterioration of concrete in hydraulic structures—interactions between water absorption, leaching and frost action. Division of Building Materials, Lund University, Sweden
89. Relling RH, Sellevold EJ (2005) In-situ moisture state of coastal concrete bridges. In: Proceedings of international conference on concrete repair, rehabilitation, and retrofitting (ICCRRR), Cape Town, p 191
90. Relling RH (1999) Coastal concrete bridges, moisture state, chloride permeability and aging effects. PhD thesis. Norwegian University of Science and Technology (NTNU). Trondheim
91. Eriksen K, Geiker MR, Grelk B, Laugesen P, Pedersen EJ, Thaulow N (1997) HETEK. Method for test of the frost resistance of high performance concrete, performance testing versus in situ observations. Report No. 93. The Danish Road Directorate
92. Samson E, Marchand J, Zuber B, Skalny JP (2002) Ettringite in air voids. In: Proceedings of international RILEM TC 186-ISA workshop on internal sulfate attack and delayed ettringite formation, Villars
93. Jakobsen UH (2016) Personal communication
94. Rosenqvist M, Bertron A, Fridh K, Hassanzadeh M (2017) Concrete alteration due to 55 years of exposure to river water: chemical and mineralogical characterization. Cem Concr Res 92:110–120
95. (1997) Durable concrete structures—design guide. Comité Euro-International du Béton
96. Alhozaimy A, Hussain RR, Al-Zaid R, Al Negheimish A (2012) Investigation of severe corrosion observed at intersection points of steel rebar mesh in reinforced concrete construction. Constr Build Mater 37:67–81
97. Jang JW, Iwasaki I (1991) Rebar corrosion under simulated concrete conditions using galvanic current measurements. Corrosion 47(11):875–884
98. The Concrete Society (1989) Spacers for reinforced concrete. Slough, UK
99. King ES, Dakin JM (2001) Specifying, detailing and achieving cover to reinforcement, CIRIA C568. Construction Industry Research and Information Association, London
100. Shaw C (2007) Cover to reinforcement: getting it right. Struct Eng 31–35
101. American Concrete Institute (1999) ACI 315-99—details and detailing of concrete reinforcement
102. (2004) ACI SP-66: ACI detailing manual. American Concrete Institute
103. (2011) DIN EN 13670:2011-03—Execution of concrete structures (German version of EN 13670)
104. Alzyoud S, Wong HS, Buenfeld NR (2016) Influence of reinforcement spacers on mass transport properties and durability of concrete structures. Cem Concr Res 87:31–44
105. (2014) fib bulletin no. 75: Polymer-duct systems for internal bonded post-tensioning. Fédération Internationale du Béton (fib)
106. Hunkeler F, Matt P, Matt U, Werner R (2005) Prestressing tendons, stay cables and ground anchors—description of the systems and lessons learnt from corrosion damages.

Research report ASTRA/AGB2000/470. Swiss Federal Roads Office, Berne
107. ACI Committee 222 (2014) report on corrosion of prestressing steels (ACI 222.2R-14). American Concrete Institute (ACI), Farmington Hills
108. Suprenant BA, Malisch WR (1998) How clean must rebar be? Concr Constr (June):#C980517
109. Taber LH, Belarbi A, Richardson DN (2002) Effect of reinforcing bar contamination on steel–concrete bond during concrete construction. ACI Mater J 209:839–862
110. Fu XL, Chung DDL (1995) Linear correlation of bond strength and contact electrical-resistivity between steel rebar and concrete. Cem Concr Res 25(7):1397–1402
111. Mimura Y, Yoshitake I, Morimoto K, Hamada S (2010) Debonding and fracture between deformed bars and early-age concrete. In: Proceedings FraMCos-7—7th international conference on fracture mechanics of concrete and concrete structures, Jeju